

A carbon cloth-based lithium composite anode for high-performance lithium metal batteries

Ying Zhou^a, Yu Han^a, Hongtao Zhang^{a,b}, Dong Sui^a, Zhenhe Sun^a, Peishuang Xiao^a,
Xueting Wang^a, Yanfeng Ma^{a,b}, Yongsheng Chen^{a,b,*}

^a The Centre of Nanoscale Science and Technology and Key Laboratory of Functional Polymer Materials, State Key Laboratory and Institute of Elemento-Organic Chemistry, College of Chemistry, Nankai University, Tianjin 300071, China

^b The National Institute for Advanced Materials, Nankai University, Tianjin 300071, China

ARTICLE INFO

Keywords:

Li metal battery
Carbon cloth
Li composite anode
Dendrite-mitigation
Full cell

ABSTRACT

The two most challenging issues for Li metal based battery are infinite volume change during uneven deposition/dissolution process and the growth of Li dendrite. Therefore, the Li metal battery exhibits poor cycling life span and even the safety issue. Here we developed a facile method to prepare dendrite-mitigation Li composite electrode (Li@CC) using commercial carbon cloth as the interfacial layer between Li metal anode and the electrolyte without pre-stored Li process in carbonate-based electrolyte. The Li@CC symmetrical cells exhibit highly reduced polarization (150 mV) and stable cycling performance (> 200 cycles) at a high current density of 5 mA cm⁻². Furthermore, the Li@CC composite anode based full cell with limited Li and moderately high loading cathode exhibits longer cycling life span, better rate performance, lower and more stable polarization than that of bare Li anode. Especially, the Li@CC-Li₄Ti₅O₁₂ full cell delivers an excellent cycling performance of 700 cycles with capacity retention of over 80%, which shows dozens of times' improvement than that of full cell based on bare Li. We believe that the high performance are due to the unique characteristics of carbon cloth such as the high conductivity, enlarged surface area and intrinsic pore structure consisted of thin crystalline graphite sheets. The high performance results with the commercial available carbon cloth can not only offer a competitive approach for industry application of Li metal battery, but also be used for other metal based energy devices.

1. Introduction

Currently, the increasing demand for electric vehicles and portable devices put an urgent requirement for high energy density batteries [1–4]. Li metal is regarded as a possible ideal anode for high energy density batteries because of its extremely high capacity (3860 mA h g⁻¹) and the lowest negative electrochemical potential (– 3.040 V vs. the standard hydrogen electrode) [5–7]. However, the practical application of Li metal anode still remains many challenges [8,9]. On the one hand, Li metal is instability to react with electrolyte to form Solid Electrolyte Interphases (SEI) film [10]. Most of the formed SEI films can't bear the infinite volume change and will crack during uneven Li deposition/dissolution process. Then the fresh Li exposes and reacts with electrolyte to form new SEI. The repeated formation and crack of SEI film not only consume Li and electrolyte uncontrollably, but also increase the interface resistance [11], thus causing the rapid delayed cycling performance. On the other hand,

the uneven Li deposition/dissolution process leads to continuous growth of Li dendrite, which may result in the safety issue induced by short circuit. To address these issues and promote the practical application of Li metal anode, lots of strategies have been proposed. Many studies devoted to SEI film modifying. For example, the in-situ SEI films were developed by adjusting electrolyte additives [12–16], and the ex-situ SEI films, including fast Li⁺ conductors [17–19], 2D mechanical stable coating [20–22] and flexible polymer layer [23,24], were prepared on the surface of Li. All those in-situ and ex-situ films on Li metal anode can stabilize the interface between electrolyte and Li metal anode relatively. Besides the interface modification, many studies devoted to designing nanostructure for preventing dendrite. A conducting matrix with high specific surface area (SSA) [25–29], polar functional groups or lithiophilic sites [30–35] can restrain the growth of Li dendrite by reducing the effective current density and guiding an uniform Li⁺ flux or inducing an inhomogeneous Li nucleation, respectively. But for practical

* Correspondence to: The Centre of Nanoscale Science and Technology and Key Laboratory of Functional Polymer Materials, State Key Laboratory and Institute of Elemento-Organic Chemistry, College of Chemistry, Nankai University, Tianjin 300071, China.

E-mail address: yschen99@nankai.edu.cn (Y. Chen).

<https://doi.org/10.1016/j.ensm.2018.04.006>

Received 4 February 2018; Received in revised form 3 April 2018; Accepted 6 April 2018

Available online 06 April 2018

2405-8297/ © 2018 Published by Elsevier B.V.

application, most nanostructural host coated on copper have to pre-store Li by an extra electrochemical deposition process, which is complicated and time-consuming. Moreover, Li composite anode has been fabricated to solve the inherent volume change issue of Li metal electrode. These include using 3D skeletons such as reduced graphene oxide (r-GO) paper with nano gaps [36], carbonized polyacrylonitrile (PAN) fiber [37], polyimide (PI) fiber [38] and carbonized 3D wood [39] with suitable microstructure to pre-store Li by thermal infusion method. The lithiophilic 3D skeletons with stable dimension and suitable pore structure restrict the volume change of Li and guide a homogeneous Li deposition without dendrite. But this method requests for sophisticated microstructure and complicated preparation process. Therefore, for practical application, it is important to develop a large-scale method to prepare a high-performance Li composite anode for mitigating the volume change and avoiding the dendrite.

In this work, we demonstrated a facile method to prepare high-performance and dendrite-mitigation Li composite electrode (Li@CC) using a commercial available material of carbon cloth (CC) without pre-stored Li process. The unique structure and morphology of CC with high conductivity and enlarged surface area facilitate the efficient charge transfer and reduce the effect current density, respectively, which are benefit for restraining the growth of dendrite at a higher current density. Also, its intrinsic pore structure consisted of thin crystalline graphite sheets as the pore walls can not only alleviate the volume change during Li deposition/dissolution process, but also introduce lithium storage mechanism with Li insertion/extraction path. As a result, the Li@CC symmetrical cells exhibit highly reduced polarization of 180 mV and stable cycling more than 200 cycles at a high current density of 5 mA cm⁻² using carbonate-based electrolyte. Meanwhile, the Li@CC anode based full cells with both Li₄Ti₅O₁₂ (LTO) and LiNi₅Co₂Mn₃O₄ (NCM) cathode exhibit longer cycling life span, significantly better rate performance and lower polarization than that of bare Li anode. Especially, the Li@CC-LTO full cell shows an excellent cycling performance exceeding 700 cycles with capacity retention of over 80% at a high current density of 2.03 mA cm⁻², while the capacity of bare Li-LTO full cell decays almost close to zero after only 40 cycles. We wish the favorable performance results with the commercial availability CC could offer a competitive approach for industry application of Li metal battery.

2. Experiment sections

2.1. Cells fabrication

The CC was used as received. Li@CC electrode was prepared by pressing a stack of CC on the top Li foil with a pressure of 10 MPa in a stainless steel mold. After that, it was tailored into disk with the diameter of 10 mm. Li foil with the thickness of 200 μm was used for symmetrical cells and Li foil with the thickness of 50 μm was used for full cells. Li mass fraction and theoretical specific capacity of fabricated Li@CC electrodes were listed in Table S1.

Two identical Li@CC electrodes and bare Li electrodes were used to fabricate the Li@CC and bare Li symmetrical cells, respectively. And for the full cells fabrication, Li₄Ti₅O₁₂ (LTO) cathode coated on Al current collector was used as received. The proportion of LTO is 90 wt%. To fabricate LiNi₅Co₂Mn₃O₄ (NCM) cathode, NCM powder was mixed with polyvinylidene fluoride (PVDF) and super-P at a weight ratio of 8:1:1. The obtained homogeneous slurry was coated on Al current collector. Then the electrode sheet was heated at 60 °C for 3 h and 150 °C for 1 h under vacuum. Both of the LTO and NCM sheets were pressed and tailored into disk with the diameter of 10 mm. The average mass loading of LTO and NCM is 12 mg cm⁻² and 11.8 mg cm⁻², respectively.

2.2. Material characterization

Scanning electron microscopy (SEM) images were taken on a PhenomPro SEM system. The cycled electrode samples for SEM characterization were first disassembled from the cells and then washed with dimethyl carbonate (DMC) to remove residual electrolyte. Power X-ray diffractometer (XRD) analysis was performed on an Ultra IV, Rigaku diffractometer with Cu Kα radiation (data was collected at a scanning rate of 20° min⁻¹ in the range of 10–80°). Raman spectrum was examined with a LabRAM HR800 Raman spectrometer using laser excitation at 514.5 nm. Tensile measurements were performed by a universal tensile testing machine (CMT 4204, MTS systems (China) Co., LTD). Electrical conductivity of CC was tested by two-wire method using KEITHLEY 2400 to get the resistance value. The average value of electrical conductivity was measured at least three times. The electrical-resistance variation was recorded by KEITHLEY 2400 after bending. Before electrical conductivity and electrical resistance variation tests, the CC was cut into a strip with the dimensions of 85 mm × 16.5 mm × 0.36 mm, then the conductive adhesive was coated on both ends of CC. For bending tests, the sample was fixed on a motorized positioning systems with a displacement speed of 2 mm s⁻¹.

2.3. Electrochemical measurements

Electrochemical measurements were carried out using coin-type cells. The electrolyte consisting of 1 M LiPF₆ in ethylene carbonate (EC):dimethyl carbonate (DMC):diethyl carbonate (DEC) (1:1:1 vol%) with 1 wt% vinylene carbonate (VC), 120 μL was used as received. Clegard 2325 was used as the separator. All cells were assembled in an argon-filled glovebox. The electrochemical performance was measured with two-electrode electrochemical cell by an automatic battery tester system (Land CT2001A model, Wuhan LAND Electronics.Ltd.). Electrochemical impedance spectroscopy (EIS) was measured on Autolab system (Metrohm) over the frequency ranging from 10⁻² Hz to 10⁵ Hz.

3. Results and discussion

3.1. Characterization of CC and Li@CC electrode

CC is widely commercial available (Fig. 1a), which possesses favorable mechanical strength and flexible property so that it can be coiled and folded to different shapes without destruction its integrity. A network structure of CC can be clearly observed from SEM image (Fig. 1b). A strand of carbon fibers (consisting hundreds of fibers) weave together compactly, ensuring the interconnection between fibers and the good integrity of CC. In addition, some interval and pore exist between carbon fibers. The analysis using Automatic Mercury Porosimeter (Fig. S1) indicates that the specific surface area of CC is 0.294 m² g⁻¹, the pore volume is 2.09 mL g⁻¹ and the average pore diameter is about 28 μm. The enlarged surface area and the pore structure benefit for the Li deposition process. The XRD spectrum of CC (Fig. S2 in red) shows typical graphite peak at 25.5 degree and 42 degree, which refer to the (002) plane and (101) plane of graphite carbon, respectively. The Raman spectrum (Fig. S3) exhibits typical G peak (1590 cm⁻¹) and D peak (1354 cm⁻¹) of graphite. Meanwhile, the value of I_G/I_D is 1.19, which refers to a relatively high degree graphitization [40] and good electric conductivity of CC. Besides, the in-plane electrical conductivity of CC gave a value of ~ 6.7 × 10³ S m⁻¹ using two-wire method.

To further verify the good mechanical and electrical stability of CC, the variation of electrical resistance of CC was measured under different curvature and after repeat bending cycling as shown in Figs. S4 and S5. The electrical resistance displays an obscure variation ≤ 0.65%. Besides, uniaxial tensile measurements exhibited negligible change of mechanical property for the samples of pristine CC and the CC after bending 200 times as shown in Fig. S6. These results revealed the good structural

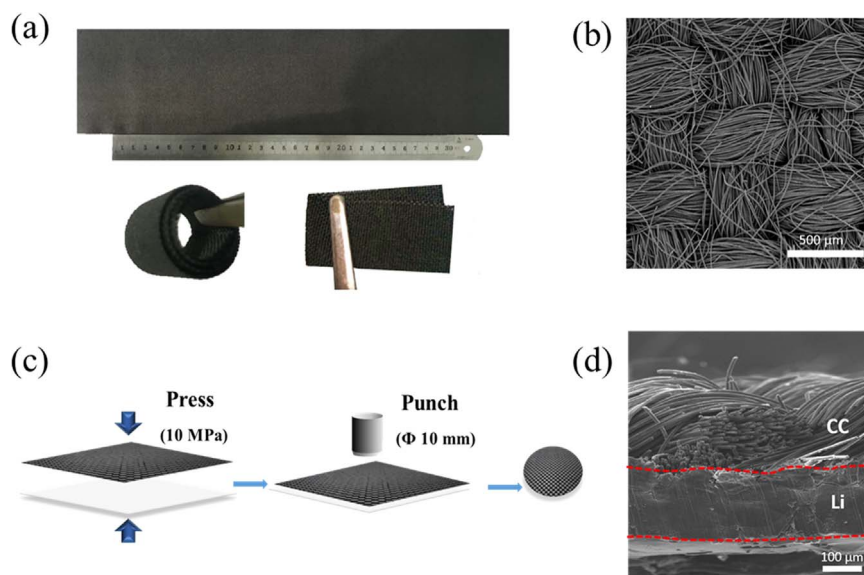


Fig. 1. (a) The optical photos of CC, it can be coiled and folded to different shapes. (b) A typical top view SEM image of CC. (c) The fabrication process of Li@CC electrode. (d) A typical cross-sectional SEM image of Li@CC electrode.

integrity and electrical conductivity stability of CC. Based on these properties of CC above, it is reasonable to believe that CC meets the needs to application in Li metal battery. With this, the Li@CC composite anode was prepared with a facile, one-step method by pressing a stack of CC on the top Li foil with a pressure of 10 MPa (Fig. 1c). The cross profiles of Li@CC (using for symmetrical cells test) revealed that the CC contacts well with bare Li (Fig. 1d). The interconnected carbon fibers as well as the well-contacted Li and CC facilitate the charge transfer process. Before the electrochemical performance investigation, the morphology change of Li@CC electrode during Li plating/stripping process was presented in Fig. S7 with cycling capacity of 2 mA h cm^{-2} using carbonate-based electrolyte. When plating at a capacity of 0.5 mA h cm^{-2} , the surface of carbon fiber show negligible morphology change, where Li insertion should be the main process (Fig. S7b1). When plating up to 1 mA h cm^{-2} (Fig. S7c1), some small Li particle deposited on the surface of carbon fiber. With further plating process, Li metal started to nucleate between fibers at a capacity of 1.5 mA h cm^{-2} (Fig. S7d1) and the size of deposited Li metal became larger without dendrite morphology at a capacity of 2 mA h cm^{-2} (Fig. S7e1). In the subsequently stripping process, the deposited Li between fibers became smaller (Fig. S7f1) and eventually disappear (Fig. S7g1), the surface of fiber became smooth and retained its initial morphology gradually (Fig. S7h1). Besides, the cross-section SEM images under all the testing with different capacity exhibited the similar morphology change as the top view SEM images, showing that the Li deposited in the CC layer uniformly with the increasing discharging capacity. After plating at capacity of 2 mA h cm^{-2} , the XRD spectrum of CC layer (Fig. S2 in blue) exhibits that comparing with the pristine CC, the (002) peak of graphite shifts from 25.5 degree to 24.5 degree and the (110) peak of Li appeared. Furthermore, the XPS spectrum of CC layer after plating was also shown in Fig. S8. The C 1s spectra exhibited the C-Li peak at 286.6 eV [41], the Li 1s spectra exhibited the Li-C peak and Li peak at 56.2 eV and 54.6 eV, respectively [11,41]. Those revealed the existence of both Li-C and Li. Therefore, the XRD and XPS results reveal the lithium storage mechanism with both Li deposition and insertion paths. Moreover, unidirectional galvanostatic plating of Li to bare CC was performed at current density of 1 mA cm^{-2} to investigate the maximum Li storage capacity according to the pristine work [26,34,35] as shown in Fig. S9. The result displayed that 137 mA h cm^{-2} Li could be plated till the short circuit of battery, exhibiting a short-circuit time (Tsc) of 137 h.

3.2. Electrochemical performances in symmetrical cells

To evaluate the performance of the Li@CC electrode, Li@CC symmetrical cells were assembled using carbonate-based electrolyte and the bare Li symmetrical cells were also fabricated as control. Fig. 2a, b and c exhibit the cycling profiles of both Li@CC and bare Li symmetrical cells at high current density of 1 mA cm^{-2} , 3 mA cm^{-2} and 5 mA cm^{-2} for 1 mA h cm^{-2} , respectively. For bare Li symmetrical cells (Fig. 2 in red color), the voltage profile exhibits a fluctuant trend and the average overpotential increases to a large value abruptly with limited cycling time. However, the Li@CC symmetrical cells (Fig. 2 in blue color) not only exhibit lower overpotential without obvious increase under the same cycling time, but also show a great improved cycling stability of over 200 cycles at high current density. This reflects the better electrode stability and transfer kinetics of Li@CC than that of bare Li. At the current density of 1 mA cm^{-2} (Fig. 2a), the bare Li symmetrical cell shows an obvious increase of overpotential, from 93 mV at the 1th cycle to over 1 V at the 160th cycle. While the Li@CC cell shows a low overpotential of about 46 mV with only 59% overpotential increase after 160 cycles. When testing at higher current density of 3 mA cm^{-2} , the bare Li cell exhibits a gradual overpotential augment after only 60 cycles, and fails after the 120th cycle. While the Li@CC symmetrical cell exhibits a lower and more stable overpotential than bare Li. Furthermore, even at high current density of 5 mA cm^{-2} , the Li@CC cell exhibits a low overpotential (150 mV) and stable cycling performance of over 200 cycles.

The electrochemical impedance spectroscopy (EIS) of symmetrical cells can also reflect the reduced polarization and more stable performance of Li@CC electrode. The semicircle at high-frequency implies the SEI interfacial resistance (R_{SEI}) and the semicircle at low-frequency implies the charge transfer resistance (R_{CT}) [19,42,43]. We define the interfacial resistance (R_{int}) as the summation of R_{SEI} and R_{CT} . Before cycling (Fig. 2d), the interfacial resistance (R_{int}) of bare Li electrode and Li@CC electrode are 139Ω and 85Ω , respectively. After the first cycle and the 50th cycle (Fig. 2e), the interfacial resistance of bare Li is 75Ω and 100Ω , respectively. While the Li@CC shows much lower interfacial resistance of 21Ω and 26Ω , respectively. The larger interfacial resistance before cycling originates from the native oxide layers on the surface of Li [36]. These results reveal that the Li@CC electrode displays a better charge transfer kinetics and more stable interface than bare Li electrode.

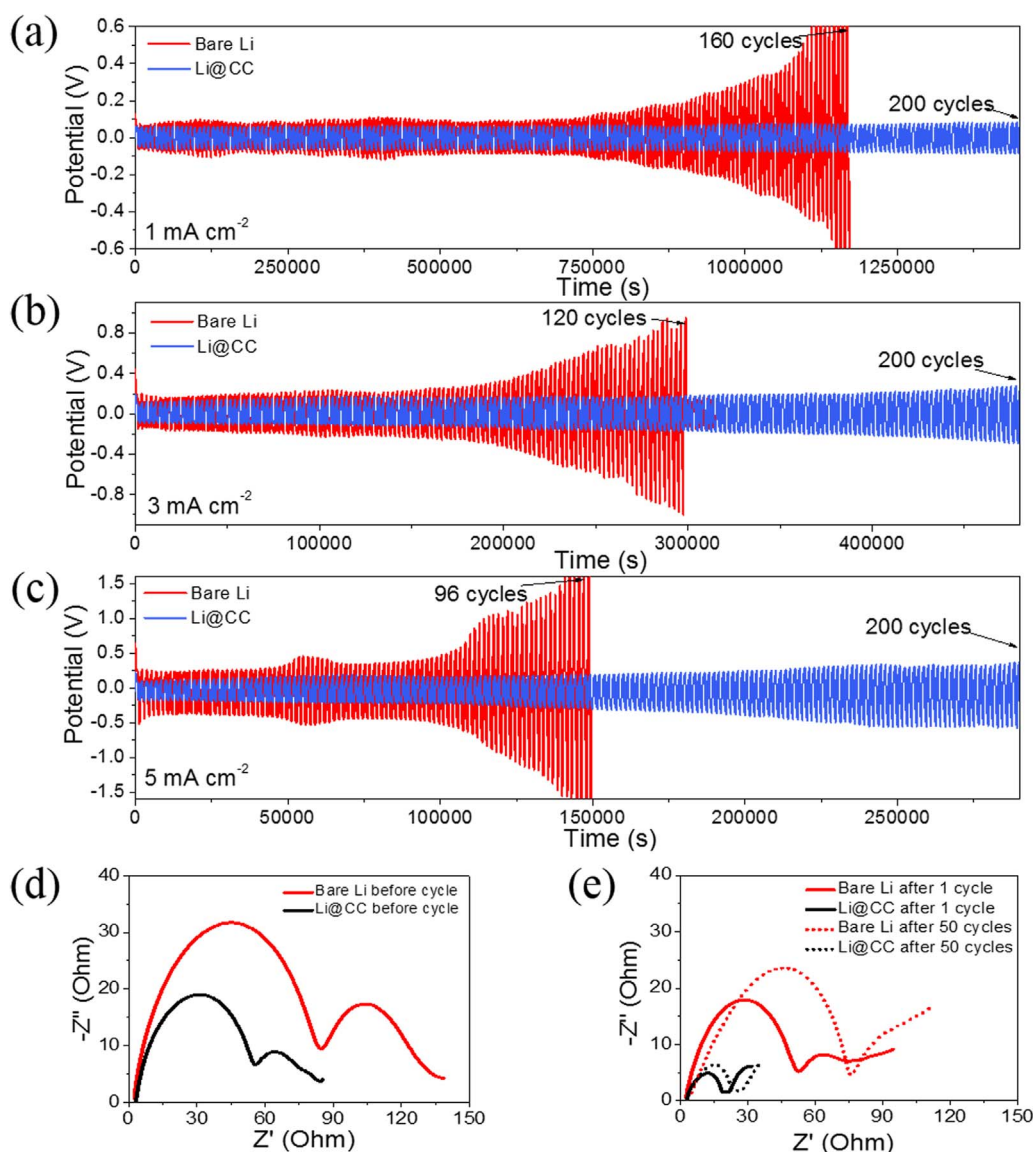


Fig. 2. The voltage profiles of bare Li symmetrical cells (red) and Li@CC symmetrical cells (blue) at different current density of (a) 1 mA cm^{-2} ; (b) 3 mA cm^{-2} , (c) 5 mA cm^{-2} . EIS of both bare Li symmetrical cell (red) and Li@CC symmetrical cell (black) (d) before galvanostatic cycle and (e) after 1th (line) and 50th (dot) galvanostatic cycles at current density of 1 mA cm^{-2} .

3.3. Electrochemical performances in full cells

To further explore the performance of Li@CC electrode, Li foil with thickness of only $50 \mu\text{m}$ was used to fabricate Li@CC anode, and LTO was used as cathode to assemble Li@CC-LTO full cells. Meanwhile, Li-LTO full cells were assembled under the same condition as control. All the Li source comes from anode. Based on the mass of Li, the Li@CC and bare Li anode offer a capacity loading of 9.1 mA h cm^{-2} . For LTO cathode, the loading mass is 12 mg cm^{-2} , corresponding to a capacity loading of $1.96 \text{ mA h cm}^{-2}$ based on the discharging capacity at 0.1 C (0.203 mA cm^{-2}) tested below. As a result, the cathode/anode capacity ratio of the fabricated full cells is about 1:4.6. Five cycles at 0.1 C were conducted for initial activation before cycling at 1 C (2.03 mA cm^{-2}) (Fig. 3a). For the full cells, the overpotential is defined as the difference between charge voltage and discharge voltage. The typical galvanostatic discharge/charge voltage profiles (Fig. 3b and Fig. S10) exhibit a lower voltage overpotential of Li@CC-LTO cell than that of bare Li-LTO cell at different current density. For bare Li-LTO cell cycling at 1 C , the discharge capacity decays at the first cycle of 120 mA h g^{-1} , and after a short plateau at about 80 mA h g^{-1} , the capacity decays quickly and almost reaches close to zero after only about 40 cycles. While the Li@

CC-LTO cell exhibits higher discharge capacity of 143 mA h g^{-1} at the first cycle. Moreover, the cell can cycle for more than 700 cycles with the capacity retention of over 80% and the discharge capacity keeps over 115 mA h g^{-1} . After five cycles at 0.1 C , the interface resistance of Li@CC-LTO is about 38Ω (Fig. 3c), which is much lower than that of Li-LTO (146Ω). Fig. 3d shows the comparison of the overpotential tendency of the two full cells above for 100 cycles. The Li-LTO cell displays an overpotential of 398 mV at the first cycle, and then rapidly increased to a high value of 1.4 V at the 40th cycle. However, for the Li@CC-LTO cell, after 100 cycles, the overpotential is slightly increased from 336 mV to 423 mV . Moreover, the Li@CC-LTO cell consistently exhibits better rate performance than Li-LTO cell. As shown in Fig. 3e, at low rate of 0.1 C and 0.2 C , the two cells exhibit almost the same discharge capacity of 163.5 and $161.2 \text{ mA h g}^{-1}$ respectively. While the capacity difference becomes obvious with increased rate. The two cells were consecutively cycled at 0.5 C , 0.75 C , 1 C and 1.5 C . The discharge capacity of bare Li-LTO cell is 155 , 145.5 , 118.5 , and 60.2 mA h g^{-1} , respectively, while the Li@CC-LTO cell shows much higher discharge capacity value of 156.5 , 152.7 , 144.7 , and $104.6 \text{ mA h g}^{-1}$, respectively.

To further verify the generality towards cathode materials of our Li@CC electrode, NCM of 11.8 mg cm^{-2} was used to assemble full cells

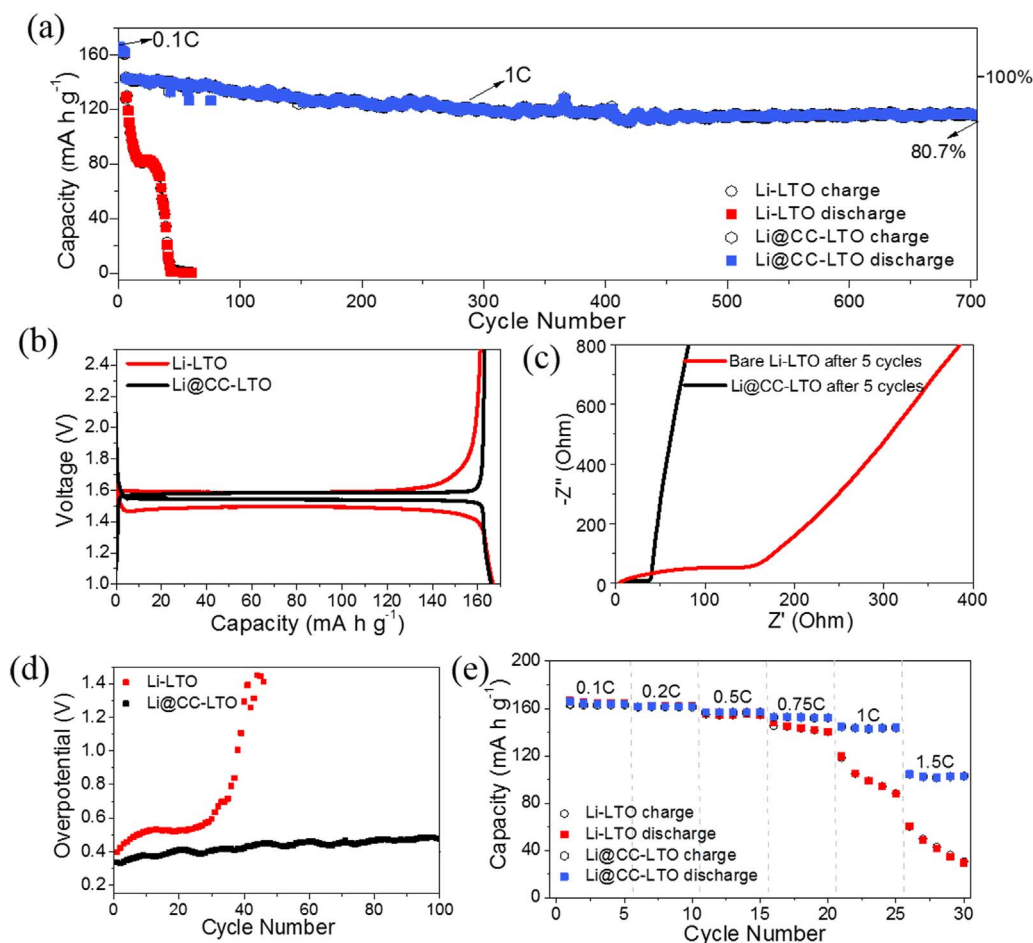


Fig. 3. (a) The cycling performance of Li-LTO cell (red) and Li@CC-LTO cell (blue). (b) The typical galvanostatic discharge/charge voltage profiles of Li-LTO cell (red) and Li@CC-LTO cell (black) at 0.1 C. (c) EIS of Li-LTO cell (red) and Li@CC-LTO cell (black) after five cycles at 0.1 C. (d) The overpotential of both Li-LTO cell (red) and Li@CC-LTO cell (black) at 1 C. (e) The rate performance of Li-LTO cell (red) and Li@CC-LTO cell (blue).

with Li@CC and bare Li anode which possessing a capacity loading of $2.12 \text{ mA h cm}^{-2}$ based on the discharging capacity at 0.1 C (0.172 mA cm^{-2} , $1 \text{ C} = 145 \text{ mA h g}^{-1}$). Therefore, the cathode/anode capacity ratio is about 1:4.3. Besides, the NCM also provides a part of Li source itself. Five cycles under 0.1 C were conducted for initial activation before cycling at 1 C (1.72 mA cm^{-2}) (Fig. 4a). The typical galvanostatic discharge/charge voltage profiles (Fig. 4b and Fig. S11) also reflect the lower voltage overpotential of Li@CC-NCM cell than that of Li-NCM cell at different current density. For bare Li-NCM cell, the capacity starts to decay rapidly only after about 40 cycles, and decreases close to zero after 75 cycles. In contrast, the Li@CC-NCM cell exhibits an excellent cycling performance at 1 C for 300 cycles with capacity retention of over 80%. Similarly, Fig. 4c exhibits the ever-increasing overpotential of Li-NCM cell (from 174 mV at the first cycle to 1.16 V at the 100th cycle) and the relatively stable overpotential of Li@CC-NCM cell (from 161 mV at the first cycle to 255 mV at the 100th cycle) during cycling. Besides, the Li@CC-NCM cell also displays higher discharge capacity at different rate than that of Li-NCM cell (Fig. 4d). Especially, the Li@CC-NCM cell exhibits a high capacity ($\sim 120 \text{ mA h g}^{-1}$) at 2 C.

To further understand the excellent performance of Li@CC-based cell, Li@CC-LTO full cell was used for further investigating with the bare Li-LTO cell as control. For the bare Li-LTO cell, Li anode and LTO cathode (after 40 cycles at 1 C) were re-assembled with new LTO cathode and new Li cathode, respectively. The cell assembled with cycled-Li and new LTO exhibits a capacity close to zero at 0.1 C (Fig. S12). In contrast, the capacity is recovered to $164.5 \text{ mA h g}^{-1}$ when the cell was assembled with cycled-LTO and new Li (Fig. S13).

These results demonstrate that the Li anode is the reason for the degradation of Li-LTO cell.

SEM was used to further characterize the morphology change of Li@CC and bare Li anode. After 5 cycles at 0.1 C, some small cracks and dendrite were observed on the surface of bare Li (Fig. S14a and S14b). While for the Li@CC anode, Li metal deposited on the surface of fibers and in the space between the fibers, and no dendrite was observed (Fig. S14c and S14d). Moreover, after 40 cycles at 1 C, for the Li-LTO cell, large cracks and much dendrite appeared on the surface of Li anode (Fig. 5a). And before cycling, the thickness of compact Li is only $50 \mu\text{m}$ (Fig. 5b). After cycling, the compact Li becomes loose completely with an increased thickness of $\sim 175 \mu\text{m}$ (Fig. 5c). The above results are consistent with the previous report [11] and indicate that the uncontrollable growth of dendrite and the accumulation of loose inactive layer are the origin of the increased internal resistance and the rapid decayed capacity of Li-LTO cell. In contrast, for the Li@CC-LTO cell, the top view SEM image of Li@CC anode shows that the Li metal deposited on the surface of fibers and in the space between fibers compactly without obvious dendrite after 40 cycles (Fig. 5d). Besides, for Li@CC-LTO cell, there was still some Li metal film underneath the CC remained after 40 cycles (Fig. 5f and Fig. S15). These results reveal that the Li@CC electrode exhibits a more stable property with good dendrite mitigating effect than bare Li electrode.

A proposed degradation mechanism of bare Li electrode is shown in Fig. 6 (left) [11,42,43]. The surface nature of Li foil (as shown in Fig. S16) and heterogeneous property of SEI could induce an uneven Li deposition/dissolution process and therefore the uncontrollable growth

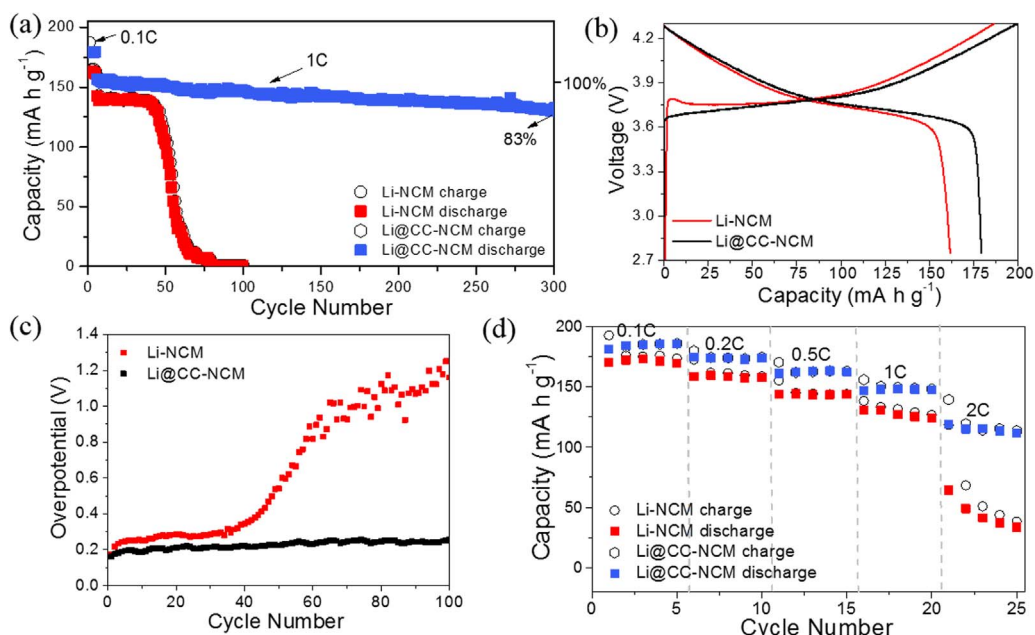


Fig. 4. (a) The cycling performance of Li-NCM cell (red) and Li@CC-NCM cell (blue). (b) The typical galvanostatic discharge/charge voltage profiles of Li-NCM cell (red) and Li@CC-NCM cell (black) at 0.1 C. (c) The overpotential of both Li-NCM cell (red) and Li@CC-NCM cell (black) at 1 C. (d) The rate performance of Li-NCM cell (red) and Li@CC-NCM cell (blue).

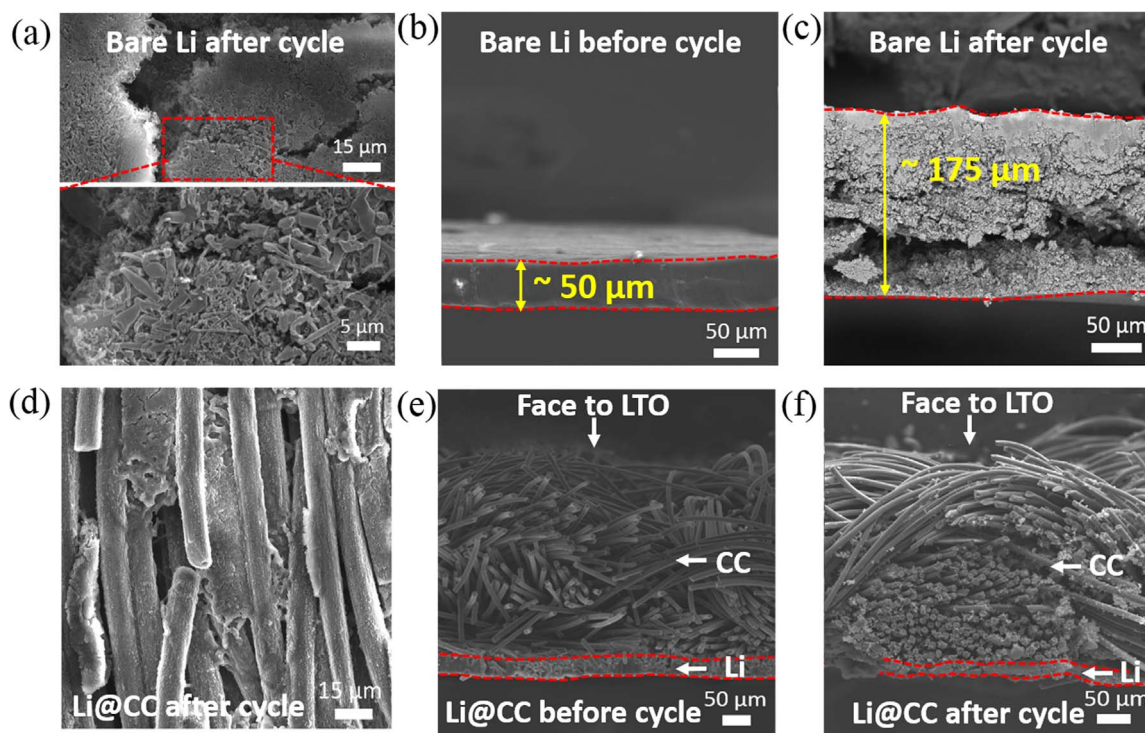


Fig. 5. Top view SEM images of (a) bare Li anode and (d) Li@CC anode in full cells after 40 cycles. Cross-sectional SEM images of bare Li anode (b) before cycle, (c) after 40 cycles and Li@CC anode (e) before cycle, (f) after 40 cycles.

of Li dendrite. The cracked SEI film caused by the volume change exposes fresh Li to react with electrolyte repeatedly. Meanwhile, the electrochemically inactive layer accumulates gradually. As a result, the interface resistance increases and the capacity declines.

In contrast, the improved cycling performance of the Li@CC electrode can be attributed to the unique characteristics of CC discussed above (Fig. 6 right). Firstly, CC possesses high electronic conductivity and enlarged surface area that facilitate the charge transfer and reduce the effect current density. As a result, our Li@CC

electrode guides a uniform Li deposition/dissolution process without obvious dendritic morphology and therefore displays a lower polarization and better stability under higher current density than bare Li. Secondly, the pore structure can alleviate the volume change by reserving Li on the surface of fibers and in the space between fibers and keep its structural integrity simultaneously. Thirdly, the unique structure of CC consisted of thin crystalline graphite sheets could make Li storage mechanism happen in the modes of both Li deposition and Li insertion.

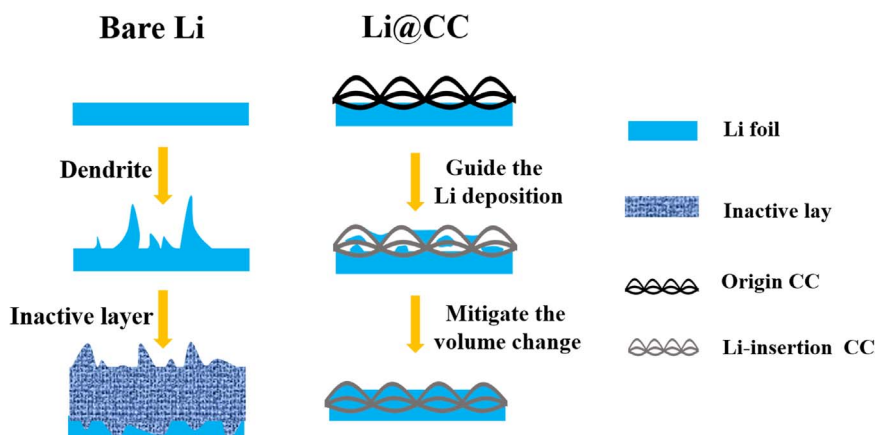


Fig. 6. The schematic of degradation of bare Li electrode (left) and the improved cycling performance mechanism of Li@CC electrode (right).

4. Conclusions

In conclusion, a low-cost and commercial available CC was used to fabricate Li@CC composite electrode by a facile one-step method. Based on the unique characteristics of CC such as the high electrical conductivity, enlarged surface area, intrinsic pore structure, the Li@CC electrode displays dendrite-mitigation property. The Li@CC symmetrical cells exhibit low polarization and stable cycling for over 200 cycles even at a high current density of 5 mA cm^{-2} . Also, the Li@CC-LTO/NCM full cells exhibit longer cycling life span at a high current density, better rate performance and lower overpotential than bare Li-LTO/NCM full cells. Especially, the Li@CC-LTO cell can cycle for 700 cycles with a capacity retention of over 80%. We believe that the excellent performance of the Li@CC electrode using commercial CC could make our approach competitive for the true industry application of Li metal battery.

Acknowledgements

This work was supported by the Ministry of Science and Technology of China (2016YFA0200200), the National Natural Science Foundation of China (51633002, 51472124, and 21421001), 111 Project (B12015), and TianJin Municipal Science and Technology Commission (16ZXCLGX00100).

Appendix A. Supporting information

Supplementary data associated with this article can be found in the online version at doi:10.1016/j.ensm.2018.04.006.

References

- [1] D. Lin, Y. Liu, Y. Cui, Reviving the lithium metal anode for high-energy batteries, *Nat. Nanotechnol.* 12 (2017) 194–206.
- [2] J. Liang, Z.H. Sun, F. Li, H.M. Cheng, Carbon materials for Li-S batteries: functional evolution and performance improvement, *Energy Storage Mater.* 2 (2016) 76–106.
- [3] Y.-Z. Sun, J.-Q. Huang, C.-Z. Zhao, Q. Zhang, A review of solid electrolytes for safe lithium-sulfur batteries, *Sci. China Chem.* 60 (2017) 1508–1526.
- [4] X. Yang, L. Zhang, F. Zhang, Y. Huang, Y. Chen, Sulfur-infiltrated graphene-based layered porous carbon cathodes for high-performance lithium-sulfur batteries, *ACS Nano* 8 (2014) 5208–5215.
- [5] W. Xu, J. Wang, F. Ding, X. Chen, E. Nasybulin, Y. Zhang, J.-G. Zhang, Lithium metal anodes for rechargeable batteries, *Energy Environ. Sci.* 7 (2014) 513–537.
- [6] J. Lang, L. Qi, Y. Luo, H. Wu, High performance lithium metal anode: progress and prospects, *Energy Storage Mater.* 7 (2017) 115–129.
- [7] X.-B. Cheng, R. Zhang, C.-Z. Zhao, Q. Zhang, Toward safe lithium metal anode in rechargeable batteries: a review, *Chem. Rev.* 117 (2017) 10403–10473.
- [8] J.M. Tarascon, M. Armand, Issues and challenges facing rechargeable lithium batteries, *Nature* 414 (2001) 359–367.
- [9] H. Li, X. Xu, R & D vision and strategies on solid lithium batteries, *Energy Storage Sci. Technol.* 5 (2016) 607–614.
- [10] X.B. Cheng, R. Zhang, C.Z. Zhao, F. Wei, J.G. Zhang, Q. Zhang, A review of solid electrolyte interphases on lithium metal anode, *Adv. Sci.* 3 (2016) 1500213.
- [11] D. Lu, Y. Shao, T. Lozano, W.D. Bennett, G.L. Graff, B. Polzin, J. Zhang, M.H. Engelhard, N.T. Saenz, W.A. Henderson, P. Bhattacharya, J. Liu, J. Xiao, Failure mechanism for fast-charged lithium metal batteries with liquid electrolytes, *Adv. Energy Mater.* 5 (2015) 1400993.
- [12] W. Li, H. Yao, K. Yan, G. Zheng, Z. Liang, Y.M. Chiang, Y. Cui, The synergetic effect of lithium polysulfide and lithium nitrate to prevent lithium dendrite growth, *Nat. Commun.* 6 (2015) 7436.
- [13] S. Xiong, K. Xie, Y. Diao, X. Hong, Characterization of the solid electrolyte interphase on lithium anode for preventing the shuttle mechanism in lithium-sulfur batteries, *J. Power Sources* 246 (2014) 840–845.
- [14] C. Yan, X.-B. Cheng, C.-Z. Zhao, J.-Q. Huang, S.-T. Yang, Q. Zhang, Lithium metal protection through in-situ formed solid electrolyte interphase in lithium-sulfur batteries: the role of polysulfides on lithium anode, *J. Power Sources* 327 (2016) 212–220.
- [15] E. Markevich, K. Fridman, R. Sharabi, R. Elazari, G. Salitra, H.E. Gottlieb, G. Gershtinsky, A. Garsuch, G. Semrau, M.A. Schmidt, Amorphous columnar silicon anodes for advanced high voltage lithium ion full cells: dominant factors governing cycling performance, *J. Electrochem. Soc.* 160 (2013) A1824–A1833.
- [16] F. Ding, W. Xu, G.L. Graff, J. Zhang, M.L. Sushko, X. Chen, Y. Shao, M.H. Engelhard, Z. Nie, J. Xiao, X. Liu, P.V. Sushko, J. Liu, J.G. Zhang, Dendrite-free lithium deposition via self-healing electrostatic shield mechanism, *J. Am. Chem. Soc.* 135 (2013) 4450–4456.
- [17] N.W. Li, Y.X. Yin, C.P. Yang, Y.G. Guo, An artificial solid electrolyte interphase layer for stable lithium metal anodes, *Adv. Mater.* 28 (2016) 1853–1858.
- [18] Y. Liu, D. Lin, P.Y. Yuen, K. Liu, J. Xie, R.H. Dauskardt, Y. Cui, An artificial solid electrolyte interphase with high Li-ion conductivity, mechanical strength, and flexibility for stable lithium metal anodes, *Adv. Mater.* 29 (2017) 1605531.
- [19] M. Baloch, D. Shanmukaraj, O. Bondarchuk, E. Bekaert, T. Rojo, M. Armand, Variations on Li_3N protective coating using ex-situ and in-situ techniques for Li^+ in sulphur batteries, *Energy Storage Mater.* 9 (2017) 141–149.
- [20] A.C. Kozen, C.-F. Lin, A.J. Pearce, M.A. Schroeder, X. Han, L. Hu, S.-B. Lee, G.W. Rubloff, M. Noked, Next-generation lithium metal anode engineering via atomic layer deposition, *ACS Nano* 9 (2015) 5884–5892.
- [21] L. Wang, L. Zhang, Q. Wang, W. Li, B. Wu, W. Jia, Y. Wang, J. Li, H. Li, Long lifespan lithium metal anodes enabled by Al_2O_3 sputter coating, *Energy Storage Mater.* 10 (2018) 16–23.
- [22] K. Yan, H.W. Lee, T. Gao, G. Zheng, H. Yao, H. Wang, Z. Lu, Y. Zhou, Z. Liang, Z. Liu, S. Chu, Y. Cui, Ultrathin two-dimensional atomic crystals as stable interfacial layer for improvement of lithium metal anode, *Nano Lett.* 14 (2014) 6016–6022.
- [23] K. Liu, A. Pei, H.R. Lee, B. Kong, N. Liu, D. Lin, Y. Liu, C. Liu, P.C. Hsu, Z. Bao, Y. Cui, Lithium metal anodes with an adaptive "solid-liquid" interfacial protective layer, *J. Am. Chem. Soc.* 139 (2017) 4815–4820.
- [24] G. Zheng, C. Wang, A. Pei, J. Lopez, F. Shi, Z. Chen, A.D. Sendek, H.-W. Lee, Z. Lu, H. Schneider, M.M. Safont-Sempere, S. Chu, Z. Bao, Y. Cui, High-performance lithium metal negative electrode with a soft and flowable polymer coating, *ACS Energy Lett.* 1 (2016) 1247–1255.
- [25] R. Zhang, X.B. Cheng, C.Z. Zhao, H.J. Peng, J.L. Shi, J.Q. Huang, J. Wang, F. Wei, Q. Zhang, Conductive nanostructured scaffolds render low local current density to inhibit lithium dendrite growth, *Adv. Mater.* 28 (2016) 2155–2162.
- [26] C.P. Yang, Y.X. Yin, S.F. Zhang, N.W. Li, Y.G. Guo, Accommodating lithium into 3D current collectors with a submicron skeleton towards long-life lithium metal anodes, *Nat. Commun.* 6 (2015) 8058.
- [27] Q. Yun, Y.B. He, W. Lv, Y. Zhao, B. Li, F. Kang, Q.H. Yang, Chemical dealloying derived 3D porous current collector for Li metal anodes, *Adv. Mater.* 28 (2016) 6932–6939.
- [28] L.L. Lu, J. Ge, J.N. Yang, S.M. Chen, H.B. Yao, F. Zhou, S.H. Yu, Free-standing copper nanowire network current collector for improving lithium anode performance, *Nano Lett.* 16 (2016) 4431–4437.
- [29] X.B. Cheng, H.J. Peng, J.Q. Huang, R. Zhang, C.Z. Zhao, Q. Zhang, Dual-phase

- lithium metal anode containing a polysulfide-induced solid electrolyte interphase and nanostructured graphene framework for lithium-sulfur batteries, *ACS Nano* 9 (2015) 6373–6382.
- [30] Z. Liang, G. Zheng, C. Liu, N. Liu, W. Li, K. Yan, H. Yao, P.C. Hsu, S. Chu, Y. Cui, Polymer nanofiber-guided uniform lithium deposition for battery electrodes, *Nano Lett.* 15 (2015) 2910–2916.
- [31] X.B. Cheng, T.Z. Hou, R. Zhang, H.J. Peng, C.Z. Zhao, J.Q. Huang, Q. Zhang, Dendrite-free lithium deposition induced by uniformly distributed lithium ions for efficient lithium metal batteries, *Adv. Mater.* 28 (2016) 2888–2895.
- [32] R. Zhang, X.R. Chen, X. Chen, X.B. Cheng, X.Q. Zhang, C. Yan, Q. Zhang, Lithiophilic sites in doped graphene guide uniform lithium nucleation for dendrite-free lithium metal anodes, *Angew. Chem. Int. Ed.* 56 (2017) 7764–7768.
- [33] L. Liu, Y.X. Yin, J.Y. Li, S.H. Wang, Y.G. Guo, L.J. Wan, Uniform lithium nucleation/growth induced by lightweight nitrogen-doped graphitic carbon foams for high-performance lithium metal anodes, *Adv. Mater.* (2018) 1706216.
- [34] C. Jin, O. Sheng, J. Luo, H. Yuan, C. Fang, W. Zhang, H. Huang, Y. Gan, Y. Xia, C. Liang, 3D lithium metal embedded within lithiophilic porous matrix for stable lithium metal batteries, *Nano Energy* 37 (2017) 177–186.
- [35] C. Jin, O. Sheng, Y. Lu, J. Luo, H. Yuan, W. Zhang, H. Huang, Y. Gan, Y. Xia, C. Liang, Metal oxide nanoparticles induced step-edge nucleation of stable Li metal anode working under an ultrahigh current density of 15 mA cm⁻², *Nano Energy* 45 (2018) 203–209.
- [36] D. Lin, Y. Liu, Z. Liang, H.W. Lee, J. Sun, H. Wang, K. Yan, J. Xie, Y. Cui, Layered reduced graphene oxide with nanoscale interlayer gaps as a stable host for lithium metal anodes, *Nat. Nanotechnol.* 11 (2016) 626–632.
- [37] Z. Liang, D. Lin, J. Zhao, Z. Lu, Y. Liu, C. Liu, Y. Lu, H. Wang, K. Yan, X. Tao, Composite lithium metal anode by melt infusion of lithium into a 3D conducting scaffold with lithiophilic coating, *Proc. Natl. Acad. Sci. USA* 113 (2016) 2862–2867.
- [38] Y. Liu, D. Lin, Z. Liang, J. Zhao, K. Yan, Y. Cui, Lithium-coated polymeric matrix as a minimum volume-change and dendrite-free lithium metal anode, *Nat. Commun.* 7 (2016) 10992.
- [39] Y. Zhang, W. Luo, C. Wang, Y. Li, C. Chen, J. Song, J. Dai, E.M. Hitz, S. Xu, C. Yang, High-capacity, low-tortuosity, and channel-guided lithium metal anode, *Proc. Natl. Acad. Sci. USA* 114 (2017) 3584–3589.
- [40] T.T. Zuo, X.W. Wu, C.P. Yang, Y.X. Yin, H. Ye, N.W. Li, Y.G. Guo, Graphitized carbon fibers as multifunctional 3D current collectors for high areal capacity Li anodes, *Adv. Mater.* 29 (2017) 1700389.
- [41] Z.Z. Tao, H. Jing, W.G. Jie, A.X. Ping, Y.H. Xi, Study on mechanism of Li-ion intercalating into carbon of graphite anode, *J. South China Univ. Technol.* (1998) 46–49.
- [42] M.-H. Ryou, D.J. Lee, J.-N. Lee, Y.M. Lee, J.-K. Park, J.W. Choi, Excellent cycle life of Lithium-metal anodes in Lithium-ion batteries with mussel-inspired polydopamine-coated separators, *Adv. Energy Mater.* 2 (2012) 645–650.
- [43] M.-H. Ryou, Y.M. Lee, Y. Lee, M. Winter, P. Bieker, Mechanical surface modification of lithium metal: towards improved Li metal anode performance by directed Li plating, *Adv. Funct. Mater.* 25 (2015) 834–841.